MFN= 006842
01 SID/SCD
02 8033
03 INPE-8033-PRE/3851
04 SRE
05 M
06 am
10 Brent, N.H.
10 Kaufman, Y.I.
10 Setzer, Alberto Waingort
10 Tanre, D.D.
10 Ward, D.E.
12 Optical properties of aerosol emissions from biomass burning in the tropics
14 403-411
16 Levine, Joel S., ed.
18 Global Biomass burning-atmospheric, climatic and biospheric implications.
20 9
40 En
41 En
42 <E>
58 DSM
62 MIT Press
64 <1991>
66 Cambridge
68 PRE
76 ESTUDOS INTEGRADOS DO MEIO AMBIENTE
83 The optical properties of smoke aerosol are discussed in the general context of biomass burning. Biomass burning in the tropics, a large source of trace gases, has expanded drastically in the last decade due to increases in the controlled and uncontrolled deforestation in South America (Tucker et al., 1984 Malingreau and Tucker, 1988; Setzer et al., 1988; Setzer and Pereira, 1989) and due to increases in cultivated areas associated with expansion of population in Africa and South America (Seiler and Crutzen, 1980). Trace gases and particulates are emitted to the atmosphere from the burning process. The biomass burning process is linked to the need to understand the sources and sinks of the atmospheric trace gases and their atmospheric variations (GTC, 1986). The importance of these trace gases (in addition to CO_2) is in their greenhouse effect, which is comparable to that of CO_2 (Ramanathan et al., 1985), and in their effect on tropospheric chemistry (Crutzen, 1988).
87 BIOMASSA
87 FUMACA
87 AEROSOIS
87 DESFLORESTAMENTO
87 DESMATAMENTO
87 POLUICAO AMBIENTAL
87 EFEITO ESTUFA
88 BIOMASS
88 AEROSOLS5DEFORESTATION
88 ENVIRONMENTAL POLLUTION
88 GREENHOUSE EFFECT5
88 SMOKE
91 FDB-19950217
92 FDB-MLR

biomass burning — queimadas
Aerosols — aerosois
deforestation — desflorestamento
smoke — fumaça
enviroment pollution — poluição ambiental
greenhouse effect — efeito estufa

© 1991 Massachusetts Institute of Technology

The MIT Press
Cambridge, Massachusetts
London, England

Optical Properties of Aerosol Emissions from Biomass Burning in the Tropics, BASE-A

Brent N. Holben, Yoram J. Kaufman, Alberto W. Setzer,
Didre D. Tanre, and Darold E. Ward

The optical properties of smoke aerosol are discussed in the general context of biomass burning. Biomass burning in the tropics, a large source of trace gases, has expanded drastically in the last decade due to increases in the controlled and uncontrolled deforestation in South America (Tucker et al., 1984; Malingreau and Tucker, 1988; Setzer et al., 1988; Setzer and Pereira, 1989) and due to increases in cultivated areas associated with expansion of population in Africa and South America (Seiler and Crutzen, 1980). Trace gases and particulates are emitted to the atmosphere from the burning process. The biomass burning process is linked to the need to understand the sources and sinks of the atmospheric trace gases and their atmospheric variations (GTC, 1986). The importance of these trace gases (in addition to CO_2) is in their greenhouse effect, which is comparable to that of CO_2 (Ramanathan et al., 1985), and in their effect on tropospheric chemistry (Crutzen, 1988).

Knowledge of the optical characteristics of smoke particles is important in regard to the following two aspects. The first aspect deals with the relation between particles and gases as biomass burning products. Smoke particles are one of the emission products in the process of biomass burning. Since they are formed due to incomplete combustion, as is the case for trace gases emitted from biomass burning, their relative abundance is proportional to the abundance of trace gases (Kaufman et al., 1990a). As a result, remote sensing of smoke particles (Kaufman et al., 1990b; Ferrare et al., 1990) can be used to asses the magnitude of the emission of trace gases from biomass burning associated with deforestation in the tropics (Kaufman et al., 1990a). These remote sensing methods are based on optical characteristics of the smoke particles derived from ground-based and airborne measurements (Puschel et al., 1988; Radke et al., 1988; Kaufman et al., 1990b) as well as on analysis of satellite imagery (Kaufman et al., 1990b; Ferrare et al., 1990). The derivation of the trace gases is based on measurements of the ratios of trace gases

to particles emission rates (Ward and Hardy, 1984; Ward, 1986). To the extend of our knowledge, except for lidar measurements of the backscattering ratio (Browell et al., 1990), there are no measurements of the optical characteristics of smoke particles emitted in the tropics. In order to use smoke particles as a tracer of the emission of trace gases, the particle mean size and the resulting relation between the smoke particles' mass and their effect on the outgoing radiation have to be established.

The second aspect deals with the effect of particles on atmospheric composition and energy balance. Particles emitted from biomass burning may affect the radiation budget and boundary layer meteorology by reflecting sunlight to space and absorbing solar radiation (Coakley et al., 1983). Smoke particles are also a major source of cloud condensation nuclei (CCNs) (Squires and Twomey, 1960; Hobbs and Radke, 1969; Radke, 1989). Therefore, an increase in the aerosol concentration may cause an increase in the reflectance of thin to moderate clouds (Twomey, 1977; Coakley et al., 1987) and a decrease in the reflectance of thick clouds (Twomey, 1977). The aerosol effect for most clouds is dominated through an increase in cloud albedo. Twomey et al. (1984) suggested that the net cooling effect from increases in aerosol concentrations can be as strong as the heating effect from the increase of global CO_2 and other trace gases and thus acts in the opposite direction (Coakley et al., 1987). The net effect of increased concentration of aerosol and trace gases on the earth's energy budget is therefore not obvious. Since the number of potential CCNs generated from biomass burning is inversely proportional to the cube of the particle radius, the mean mass radius of smoke particles has to be established.

Biomass burning in the tropics is of particular interest, because of the large extent of forest clearing and agricultural burning. Estimates based on satellite imagery are of ~200,000 square kilometers (km^2) in Brazil alone (Setzer et al., 1988; Setzer and Pereira, 1989). The high solar irradiation in the tropics enhances atmospheric chemical reactions (due to ultra-

violet radiation) and the climatic effects of aerosols (more solar radiation reflected to space).

Sunphotometry has been a useful tool to measure optical properties of aerosols for many years; however, until this past decade when tropical biomass burning became a significant issue in the research community, few researchers studied the optical properties of smoke with sunphotometry. Kaufman et al. (1990b) measured aged smoke near Washington, D.C., generated from Canadian forest fires and traveling across 4000 km (Ferrare et al., 1990). In order to assess the smoke particle size from remote measurements, Kaufman et al. (1990b) measured by a sunphotometer from the ground a wavelength dependence of the aerosol optical thickness (τ_a) of $\alpha = 1.65 \pm 0.15$ (where $\alpha = d\ln \tau_a/d\ln \lambda$), and an aerosol optical thickness of $\tau_a \sim 1$ at 500 nm. This value of α indicates a mean mass radius of the particles around 0.2 μm. Pueschel et al. (1988) studied several fires in California using the Ames airborne autotracking sunphotometer. They found that the wavelength dependence of the smoke optical thickness varied with the residence time and the source of the fuel and that forest fire smoke showed a wide range of wavelength dependencies, indicating a wide range of particle size.

In this chapter, ground-based and airborne measurements of the smoke particles' optical properties are reported. The method of measurements is summarized, followed by a summary of the results of ground-based and airborne measurements and a discussion of the smoke aerosol optical model. Aerosol absorption is discussed, and measurements are reported of the effect of smoke particles on the outgoing radiation.

Method

Measuring the optical properties of smoke emissions from biomass burning in Brazil required a multitemporal and multielevational approach to characterize smoke aerosol background conditions, fresh smoke from the flaming phase, aged smoke from flaming, fresh smoke from the smoldering phase, and a mixture of all. Sunphotometers were used at ground level and in the Institute for Space Research (INPE) aircraft on 3, 4, and 6 September 1989, during prescribed fire events near Alta Floresta, Matto Grosso, in Brazil. Ground observations of mixed smoke representing background conditions were made in the mornings before the fires were started. Plume observations were made from flaming and smoldering conditions and in the case of the flaming source, observations from 10 m, 500 m, 1 km, and 10 km from the source allowed evaluation of the effects of short-term aging on the aerosols.

The airborne sunphotometer was operated through an open window of the twin-engine INPE aircraft. Profiles were made at heights from 300 m to 4000 m from the surface in approximately 600 m intervals flying in 5 km ovals such that a series of readings could be made while the sunphotometers faced the sun at a constant elevation; then the climb to the next measurement elevation could be made on the turns. We assumed constant optical depth during each 5 km transect. Profiles were made in late morning before fires were started (background mixed smoke) and mid-afternoon at the peak of burning (flaming smoke). A profile was also made in transect to Alta Floresta in the semiarid *cerrado* to characterize the aerosols from that substrate.

All sunphotometers were cross-calibrated immediately before, during, and after the BASE-A experiment. It was found that the aerosol optical thickness can be measured to a precision of ±0.02 between the three instruments and an accuracy of ±0.05. The absolute calibration used was obtained by cross-calibration with a spectrometer calibrated by viewing the sun from a tethered balloon at an altitude of 30 km. The precision of calibration between the spectral bands is estimated to be ±0.02. These relatively large uncertainties resulted from instabilities detected in one or more of the sunphotometers. In the section on airborne observation the aerosol optical thickness of the mixing layer alone is obtained from the differences between two levels, 500 m and 3500 m, which removes the absolute calibration uncertainty. Nevertheless, spatial inhomogeneities and temporal evolution of the mixing layer lead to an estimate of the precision of ±0.02 as well. These uncertainties in the precision lead to uncertainties in the derived particle size of ±0.02 μm for the mixing layer, or the whole atmosphere. The estimate of the particle size of the optically thin layer above 3.5 km is more uncertain, and we can only roughly estimate the particle size.

The airborne instrument had, in addition to 3 "aerosol" channels (at 450, 650, and 850 nm), a broad and narrow band centered in the water vapor absorption region, 0.935 to 0.950 μm. This allowed water vapor retrieval. The retrievals were compared to measured radiosondes at Dulles Airport near Washington, D.C., and found to agree within ±0.4 centimeters (cm) for total column water vapor, for a range of 1 to 5 cm of water.

The aerosol optical thickness in each spectral band is computed from the Bouguer-Lambert-Beer law—

$$V_\lambda = r^2 \times V_{0\lambda}\exp(-\tau_\lambda/\mu_o) \qquad (49.1)$$

where V_λ is the output voltage of the sunphotometer for a bandwidth λ; $V_{0\lambda}$ is the zero air mass voltage intercept at that bandpass for a mean normalized Earth-sun distance (r) of 1.00; τ_λ is the wavelength-dependent vertical optical depth above the sunphotometer; and μ_o is the cosine of the solar zenith angle at the observation site.

The wavelength dependence of the aerosol optical thickness may be computed in terms of the Ångstrom exponent α:

$$\alpha = ln(\tau_2/\tau_1)/ln(\lambda_1/\lambda_2) \qquad (49.2)$$

where λ_1 and λ_2 can be any two aerosol spectral channels.

α was modeled for spherical aerosols assuming an index of refraction of $1.43 - 0.0035i$ using Dave's Mie scattering code. Assuming that the smoke aerosol size distribution is a log normal function, a look-up table of α was computed as a function of the size distribution parameters (mean geometric radius, r_g, and the standard deviation of the natural logarithm of the radius, σ). r_g was converted to the mean mass radius and the effective radius, r_m and r_{eff}, respectively, according to

$$r_{eff} = r_g\exp(2.5\sigma^2) \text{ and } r_m = r_g\exp(1.5\sigma^2) \qquad (49.3)$$

The effective radius r_{eff} is defined as the ratio of the volume and the geometrical cross-section

$$r_{eff} = \int r^3 n\ (r)\ dr / \int r^2 n\ (r)\ dr \qquad (49.4)$$

It is an appropriate parameter for radiative computations and it is directly related to the mass radius r_m by $r_{eff} = r_m \exp(\sigma^2)$ for a log normal size distribution. We express the results also in terms of r_m, since r_m describes the median mass distribution. The derived value of r_{eff}, in contrast with r_g, does not have a strong dependence on σ. The analysis of the data showed that the spectral range of the present optical thickness observations (at wavelengths of 450 to 850 nm) is not wide enough to measure σ (see Figure 49.1). Therefore, in the following the results for r_{eff} and r_m will be given for a range of σ between 0.3 and 0.9. This range was chosen based on the size distributions measured from aircraft by Radke et al. (1978) and Stith et al. (1981). A best fit to the volume distributions in Figure 2 of Radke et al. (1978) and Figure 2 of Stith et al. (1981) results in σ in the range 0.6 to 0.8.
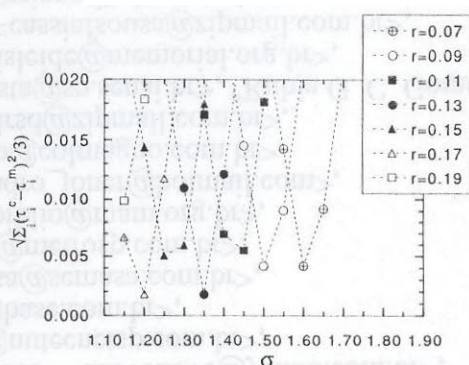

Figure 49.1 Sum of the differences between the retrieved, τ^c, and measured, τ^m, aerosol optical thicknesses for three bands (450, 650, and 850 nm) are plotted as a function of the standard deviation, σ, for several mean geometric radii r_g.

Three spectral aerosol optical thicknesses were measured allowing two independent data sets of α to be computed and were modeled for a range of effective sizes ($r_m = 0.01$ to $2.0\ \mu$m and $\sigma = 0.10$ to 2.00). The results from the ground observations are presented in terms of the size distribution under the constraints of our ability to evaluate directly the in-plume smoke particles. The aircraft observations were also interpreted for the size distribution of the mixing layer and of the atmosphere above it. Because the aircraft measured profiles of the optical thicknesses, the optical thicknesses data were converted into the extinction coefficient (km^{-1}) allowing comparisons to *in situ* aircraft measurements of trace gases and particulates within a layer. The water vapor profile is also presented.

Ground-Based Observations

Background Observations
Background observations of mixed smoke are made away from the plume and were taken on all observation days at various times. These measurements represent mixed smoke conditions, and can be used to extract the smoke properties of a particular plume from the total measurements of the optical thickness. The background optical depths increased from morning through the afternoon at all wavelengths owing to the increase of emission products introduced to the mixing layer from biomass burning. The spectral dependence of the optical thickness, α, increased during

the day from 1.5 to 2.2 indicating a decrease in the effective particle radius from 0.45 μm to 0.22 μm from the aged morning smoke to the fresher afternoon smoke (Figure 49.2). In the next section we shall show that fresh smoke had smaller particle sizes. We noted an increase in optical depth of the background conditions from 3 to 6 September; however, the trend was significant with the limited data available and did not affect α or the size distribution. We therefore used the smoothed time-dependent background values for all dates to correct our individual plume observations. This was accomplished by subtracting the background aerosol optical thicknesses from the total aerosol optical thicknesses, to result in the net plume optical thickness.

A second background correction for the measured plume optical thickness was made by subtracting the optical thicknesses measured by the aircraft above 4 km. These high atmospheric optical thicknesses were

(a)

(b)

Figure 49.2 Sunphotometer observations made during 3 and 4 September 1989 were used as background conditions for computation of alpha and the aerosol optical thickness. (a) Alpha increased from morning to afternoon and the mass radius decreased by about one-half during the same time period. (b) The aerosol optical thickness approximately doubled from late morning to late afternoon.

shown to be relatively stable through time and date from the plume observations. This resultant optical thickness characterizes a combination of the plume and mixing layer. We therefore analyzed observations for smoke from active fires in three conditions, termed "whole atmosphere," "mixing layer," and "plume." These were analyzed for flaming, smoldering, and background conditions.

Fresh Smoke

Observations of fresh smoke (approximately 5 to 10 seconds old) from the flaming phase were highly variable due to the lack of homogeneity of the plume during the 40 seconds required to make a spectral observation series. A running average of 20 observations out of the 80 observations collected continuously from a specific fire decreased the high frequency variations in the wavelength dependence of the optical thickness. No further increase in stability was noted by averaging on a larger number of observations. The results are summarized in Table 49.1. The mean mass radius r_m of the fresh smoke in the plume is $r_m = 0.15$ to 0.24 μm (for $\sigma = 0.5$ and corresponding to $\alpha = 2.1$ to 2.7); the mixing layer results in $r_m = 0.13$ to 0.22 for the plume plus boundary layer smoke and $r_m = 0.20$ to 0.27 for the whole atmosphere.

Two other data sets of slightly older smoke (~1 minute and ~5 minutes) were analyzed as the previous data set. The wavelength exponent for the plume increased with aging time from 2.8 to 3.2, with a corresponding decrease in the value of r_m for the net plume to 0.16 μm and 0.14 μm, respectively (Table 49.1). Observations of a one-hour-aged plume, approximately 10 km downwind of the source, showed a decrease in the wavelength exponent to 2.85, with a corresponding smaller particle size $r_m = 0.11$.

Smoldering Smoke

Observations of smoldering/flaming phase smoke were made of relatively fresh smoke less than one minute old. The wavelength exponent of the net plume was 3.25, resulting in no solution for r_m under the specified conditions. Decreasing σ to 0.3 yields an r_m of 0.09. Note that these data were made late in the day when no background data was measured. Therefore it is unlikely our background correction made by extrapolation is applicable.

Discussion of the Ground-Based Observations

This investigation shows that background smoke characteristics are different from fresh smoke characteristics. Therefore, background smoke observations
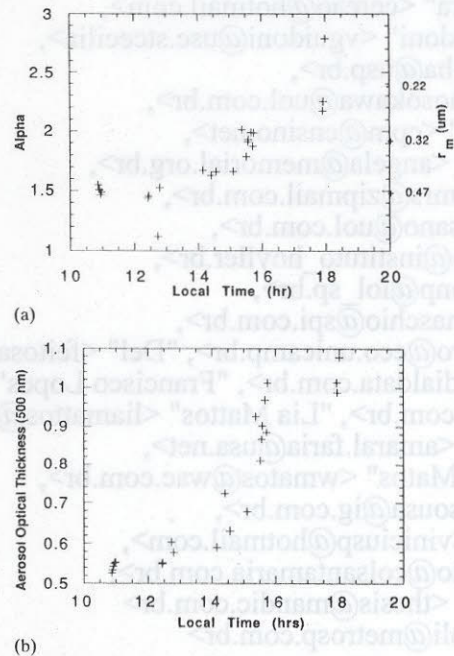
Table 49.1 Summary of ground-based measurements

Smoke type	Plume values			r_m		
	$\tau_a\ (0.50\ \mu m)$	$\alpha\ (0.50/0.875)$	Whole atmosphere	Mixed layer	Plume	
Fresh smoke (10 sec)	1.0–1.7	2.4 ± 0.3	0.20–0.27	0.13–0.22	0.14–0.24	
Less fresh smoke (1 min)	1.0–2.1	2.8 ± 0.2	0.19–0.20	0.12–0.15	0.10–0.15	
Less fresh smoke (5 min)	0.45–0.75	3.15 ± 0.05	0.20–0.22	0.11–0.15	0.07–0.09	
Aged smoke (1 hour)	1.0–1.1	2.85 ± 0.03	0.19–0.20	0.12–0.15	0.11–0.12	
Smoldering	1.7–1.9	3.25 ± 0.10	0.18–0.19	0.11	0.07 and lower	
Background smoke	0.5–1.0	1.5–2.2	0.22–0.45ª			

Note: $\tau_a\ (0.50\ \mu m)$ = the aerosol optical thickness; $\alpha(.50/.875)$ = the wavelength dependence of the optical thickness; r_m = the mean mass radius of the particles.
a. Observations taken over a range of days and burning conditions.

are critical for evaluating the optical properties of the net smoke generated from biomass burning in Brazil. Accounting for the background contribution to the smoke optical properties reduced the mean mass radius by 0.06 to 0.08 μm, or 30% to 50%. Aging of the smoke in the first hour decreased the mean mass radius for the flaming phase from 0.17 to 0.13 μm. The smoldering phase smoke indicated the smallest size distribution. However, the background correction for the smoldering phase is questionable. The decrease of the particle size within the first hour can be attributed to the deposition of larger ash particles generated in the dynamic flaming phase but not in the smoldering phase. The increase in the particle size in the next several hours (from the fresh smoke to the background smoke measured the next morning) can be due to coagulation of the liquid organic aerosol particles (Radke, private communication, 1988) and interaction with water vapor. The smoke aerosol model, which is applicable for remote sensing of fresh biomass burning, is therefore defined by a particle mean mass radius between 0.10 and 0.20 μm. The background aged smoke model would be represented by a mean mass particle radius of 0.2 to 0.4 μm. For comparison, aircraft measurements of volume size distribution made by Radke et al. (1978) and Stith et al. (1981) showed mean mass radii between 0.12 and 0.22 μm, which is similar to the present measurements.

Airborne Observations

Water Vapor Profiles

Three water vapor profiles from 3, 4, and 6 September indicated almost identical results (Figure 49.3), indicating that approximately 50% of the total water vapor is within the first km. Above 3 km the total
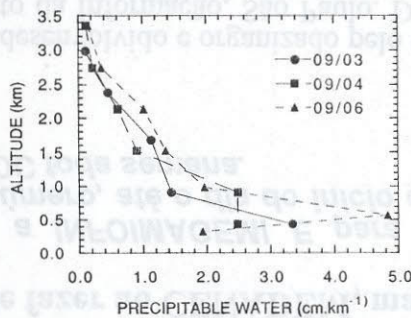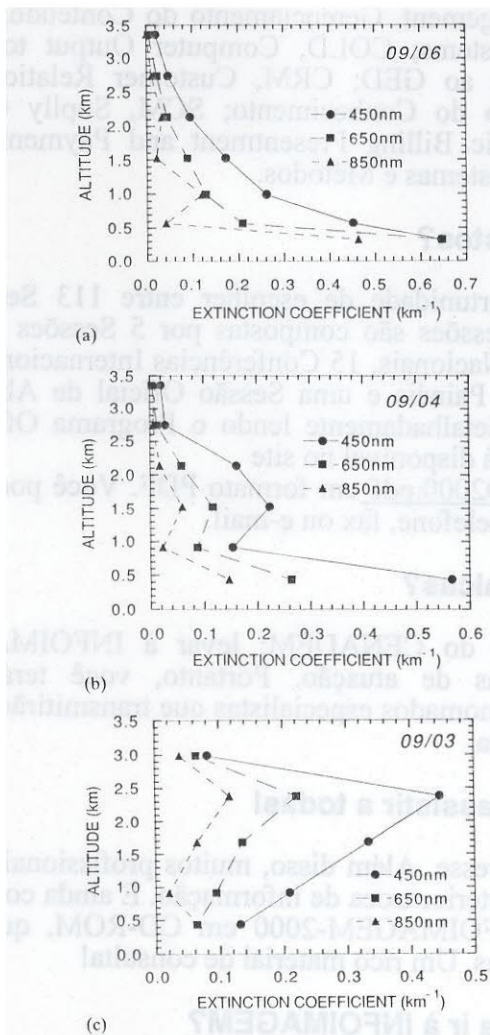
Figure 49.3 The vertical profile of the precipitable water was measured for three conditions on three dates: flaming phase (3 September), smoldering phase (4 September), and background (6 September).

precipitable water vapor is less than 0.5 cm. Because the mixing layer was below 3 km throughout the experiment, virtually all of the water in the atmosphere is available for interaction with the emission products. Note that on 6 September the high concentration of water vapor at 0.6 km is due to the presence of thin cirrus clouds.

Aerosol Profiles

Three aerosol profiles were measured corresponding to three times of the day (Figure 49.4): a 10:00 flight which we term *background condition* (6 September); a 12:00 noon flight in which the mixing layer is becoming active but with only aged (>1 day) smoke and smoke from smoldering, termed *smoldering* (4 September); and a 15:00 profile in which many flaming fires are contributing to the aerosol loading, termed *flaming* (3 September). The background profile resulted in large extinction coefficients (>0.5 km⁻¹) for all wavelengths below 500 m above ground level

ALTITUDE (km)

09/06

● 450nm
■ 650nm
▲ 850nm

EXTINCTION COEFFICIENT (km⁻¹)

(a)

ALTITUDE (km)

09/04

● 450nm
■ 650nm
▲ 850nm

EXTINCTION COEFFICIENT (km⁻¹)

(b)

ALTITUDE (km)

09/03

● 450nm
■ 650nm
▲ 850nm

EXTINCTION COEFFICIENT (km⁻¹)

(c)

Figure 49.4 The vertical profiles of the extinction coefficient measured at 450, 650, and 850 nm are plotted for (a) the background conditions, (b) the smoldering phase, and (c) the flaming phase.

(AGL). The extinction coefficients decreased exponentially with elevation to less than 0.1 km^{-1} above 2.0 km AGL (Figure 49.4a).

The smoldering phase profile indicated high extinction coefficients below 0.5 km and between 1.5 and 2.0 km with a much stronger wavelength dependence than the background conditions. Above 2.5 km the results were very similar to the background (Figure 49.4b). The flaming phase profile showed emission from of the flaming smoke directly to a layer at 2 to 3 km AGL. Thin high smoke layers were already observed in Brazil during the burning season (Andreae et al., 1988). In contrast to the other profiles, lowest extinction coefficients occurred near the ground and, like the other profiles, almost no wavelength dependence was observed for the highest layer (>3 km, Figure 49.4c).

The mean optical thickness above 3.5 km for each phase was comparable in the three days of observations: 0.13 ± 0.02 at $\lambda = 650$ nm (Table 49.2). It was less wavelength dependent in background conditions than in smoldering or flaming conditions; the corresponding effective radius r_{eff} decreased from more than 1 μm for background conditions to 0.5 μm for flaming conditions (Table 49.2).

Within the mixing layer, the optical thickness at 650 nm was 0.36 for the flaming phase, 0.26 for the smoldering phase, and 0.31 for the background smoke (see Table 49.2). The effective radius was smallest in the flaming phase (0.16) and increased to 0.20 and 0.22 for smoldering and background conditions. These results confirm the smaller particle size for fresh smoke as deduced from ground measurements.

Comparison to CO Profiles

CO samples were made during the smoldering and background profiles. The emissions of particulates and CO are highly correlated at ground levels; however, because of different dispersion rates and atmospheric lifetimes, owing to very different mass and physical properties, it is not known how well they correlate in a large convective laboratory such as the Amazon Basin. In Figure 49.5a the background extinction coefficient profile at 450 nm was plotted against the CO profile. Both demonstrate an exponential decrease in value with elevation over nearly an order of magnitude of change for each variable (Figure 49.5a). The smoldering profile also demonstrated a high degree of similarity although the correspondence was not as good as the background profile. These data suggest that remote sensing of the optical properties of the aerosols is potentially a good estimator of CO emissions under these two conditions. With

Table 49.2 Smoke aerosol optical thickness, τ; wavelength dependence, α; and particle mean mass radius, r_m for the mixing layer and the layer above 3.5 km, from aircraft measurements

Date	Smoke type	τ (0.45 μm)	τ (0.65 μm)	τ (0.85 μm)	r_{eff} (μm)
Layer above 3.5 km					
3 September 89	Flaming	0.17	0.12	0.10	≈ 0.5
4 September 89	Smoldering	0.16	0.15	0.14	≈ 1.0
6 September 89	Background	0.13	0.12	0.11	≥ 1.0
Mixing layer					
3 September 89	Flaming	0.76	0.36	0.18	0.16 ± 0.03
4 September 89	Smoldering	0.55	0.26	0.12	0.20 ± 0.03
6 September 89	Background	0.57	0.31	0.16	0.22 ± 0.03

sufficient CO-to-particulate ratios the particulate matter could be computed and compared to estimates made from optical thickness observations.

Summary of the Smoke Optical Model

Spectral measurements from the ground and from aircraft of the smoke aerosol optical thickness indicate large Ångstrom coefficients of $\alpha = 2.1$ to 2.5 except for the upper troposphere (above 3.5 km), as measured from the aircraft and during morning conditions where the measured smoke was emitted at least one day earlier ($\alpha = 0$ to 1.5). These results are in agreement with measurements conducted in North America from aircraft (Pueschel et al., 1988) and lidar backscattering in Brazil (Browell et al., 1990). Assuming a log-normal distribution of the smoke particles, with σ in the range 0.3 to 0.9 the effective radius r_{eff} for the plume is in the range 0.10 to 0.18 μm for fresh smoke, 0.10 to 0.13 μm for smoldering, and 0.2 to 0.4 μm for background aged smoke. For the whole atmospheric mixed layer, far away from the plume, the effective radius is, respectively, 0.16, 0.20, and 0.22 μm.

Single Scattering Albedo and Graphitic Carbon

The single scattering albedo measures the effectiveness of the aerosol absorption, and it depends on the refractive index and on the size distribution of the particles. Smoke aerosol is a mixture of graphitic carbon and organic particulates. The characteristics of each component are

	Organic particulates	Graphitic carbon
Refractive index	$1.43-0.0035i$	$2.00-0.66i$
Mass radius (μm)	0.15	0.03–0.10

The graphitic carbon component was taken from Ackerman and Toon (1981) and organic particulates characteristics are derived from our results.

During the BASE-A experiment, mass measurements were made only through the plume of smoke generated in the flaming stage, and 10% of the total mass was found to be graphitic carbon (Ward et al., 1990). Accounting for liquid water, 70% relative humidity consists of 50% of the particles volume (Fraser et al., 1984; Kaufman et al., 1990b), and 5% of the total particles mass is graphitic carbon. For simplicity, the volume ratio was assumed identical to mass ratio. For three intermediate mass radii within the previous range—0.03, 0.05, 0.10 μm—we computed the single scattering albedo from the Mie theory by assuming an external mixing. The results are within 0.89 to 0.91 which is more absorbing than indicated from previous remote sensing studies (Kaufman et al., 1990). Since the mass ratio of graphitic carbon was measured through the plume only, it seems reasonable to assume that it would be smaller far away from the fire.

## Application to Radiance Measurements

In this section the optical model is used to predict the difference between the upward radiance measured below the smoke layer and at the top of the smoke layer. The radiances were measured above a uniform undisturbed forest on 6 September 1989, during simultaneous measurements from the aircraft of the aerosol spectral optical thickness. The analyzed radiances were measured at 500 and 3600 m above the ground at 0.44 μm and 0.65 μm bands of a four-channel radiometer. The radiometer was calibrated in a NASA/GSFC calibration facility using an integrating sphere. Table 49.3 and Figure 49.6 summarize the radiances and optical thickness measured from the aircraft on 6 September. The radiances are normalized to reflectance units.

Since the low-level radiance was measured at 500 m

EXTINCTION COEFFICIENT K (km^{-1})

(a)

EXTINCTION COEFFICIENT K (km^{-1})
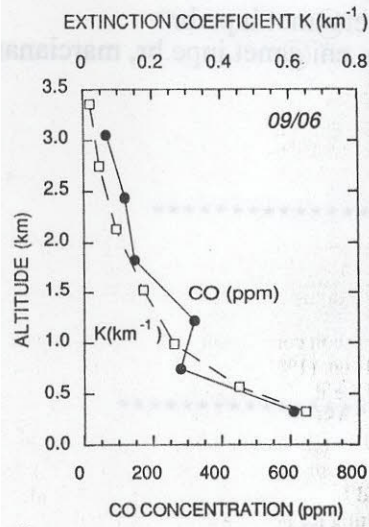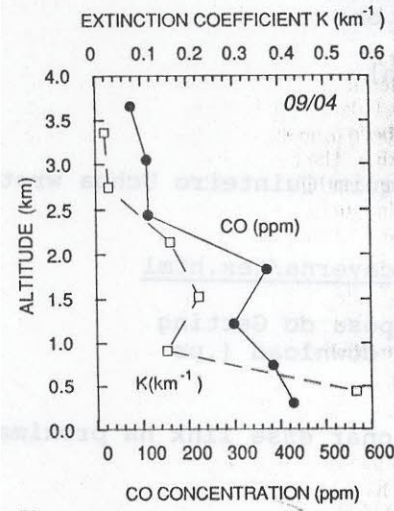
(b)

Figure 49.5 The vertical profiles of the extinction coefficient in the blue band (450 nm) and the CO concentration (ppm) are plotted for (a) the background conditions and (b) the smoldering phase.
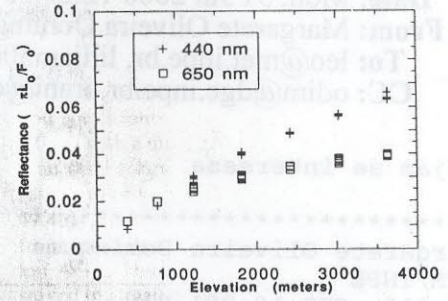

Figure 49.6 A nadir-view aircraft profile of the spectral reflectance from a closed forest canopy near Alta Floresta demonstrates an increase in atmospheric effect with altitude. Coincident sunphotometer observations allowed comparisons of the wavelength dependence of the reflectances to that of the aerosol optical thickness.

rather then at the ground, the difference in the measured optical thickness at 500 m and 3500 m (also shown in Table 49.3 for two wavelengths) was used to compute r_{eff} for this smoke layer for three values of σ. For each of the σ values in Table 49.4, the optimum value of r_{eff} was found and the predicted difference in the upward radiance was computed. As expected, for each value of σ a value of r_{eff} was found to fit the measured optical thickness with residual errors much smaller then the measurement accuracy. Surprisingly, though, the measured values of the radiance difference were not reproduced for $\sigma = 0.5$, but rather for $\sigma = 0.2$. This may be an indication that the wavelength dependence of the radiance is much more sensitive to the width of the size distribution than the wavelength dependence of the optical thickness, and that the width of the size distribution of particles emitted from biomass burning in the tropics is much smaller then the width of the distribution measured from fires in North America. This part of the investigation requires additional measurements and sensitivity analyses to establish the value of σ and its effect on the radiance.

Conclusions

Measurements of the tropical smoke aerosol optical characteristics were reported for several biomass fires and smoke conditions, as a function of time and height in the atmosphere. It was found that the wavelength dependence of the optical thickness can be explained by a log-normal size distribution with particle's effective radius varying between 0.1 and 0.2 µm. Analysis

Table 49.3   Upward radiance (in reflectance units) and corresponding aerosol optical thicknesses measured from the aircraft on 6 September 1989 for two flight altitudes

Wavelength thickness	Measured radiance		Measured aerosol optical thickness	
	500 m	3500 m	(500 m)	(3500 m)
0.44 μm	0.015 ± 0.004	0.067 ± 0.005	0.62	0.13
0.65 μm	0.018 ± 0.005	0.039 ± 0.005	0.35	0.12

Table 49.4   Comparison between the measured radiance difference between the two flights and the computed radiance difference for the measured optical thickness, and several values of the effective radius and the width of the particles size distribution σ that fit the measured wavelength dependence of the optical thickness

r_{eff}	r_m	σ	Difference in the upward radiance			
			Measured		Computed	
			450 nm	650 nm	450 nm	650 nm
0.17	0.15	0.26	0.047	0.018	0.047	0.019
0.17	0.17	0.18	0.047	0.018	0.047	0.017
0.11	0.09	0.51	0.047	0.018	0.058	0.027

of the upward radiance indicated that perhaps the width of the smoke particles size distribution is much narrower then reported from fires in North America. Surprisingly, strong sensitivity of the wavelength dependence of the upward radiance on the width (σ) of the particle size distribution generated a poor fit for σ = 0.5 but a good fit for σ = 0.2. Further measurements of the relation between the upward radiance and the smoke optical thickness are necessary to verify this finding. A strong correlation was found between the aerosol particles profile and the CO profile. This high correlation indicates that smoke particulates can be a good tracer for emission of trace gases from biomass burning in the tropics. Further investigations are also required to characterize the plume aerosols, taking better account of background conditions. Measurements of the solar aureole are required to invert into a full-size distribution. A more complete trace gas and particulate profile is required for specific burning conditions to compare with sunphotometer data profiles. Without this, remote sensing of biomass emissions will remain only an educated guess.